

Probabilistic Multisite Precipitation Downscaling by an Expanded Bernoulli–Gamma Density Network

ALEX J. CANNON

Meteorological Service of Canada, Vancouver, British Columbia, Canada

(Manuscript received 16 August 2007, in final form 30 April 2008)

ABSTRACT

A nonlinear, probabilistic synoptic downscaling algorithm for daily precipitation series at multiple sites is presented. The expanded Bernoulli–gamma density network (EBDN) represents the conditional density of multisite precipitation, conditioned on synoptic-scale climate predictors, using an artificial neural network (ANN) whose outputs are parameters of the Bernoulli–gamma distribution. Following the methodology used in expanded downscaling, predicted covariances between sites are forced to match observed covariances through the addition of a constraint to the ANN cost function. The resulting model can be thought of as a regression-based downscaling model with a stochastic weather generator component. Parameters of the Bernoulli–gamma distribution are downscaled from the synoptic-scale circulation, and unresolved temporal variability is generated via an autoregressive noise model. Demonstrated on a multisite precipitation dataset from coastal British Columbia, Canada, the EBDN is capable of specifying the conditional distribution of precipitation at each site, modeling the occurrence and the amount of precipitation simultaneously, reproducing observed spatial relationships between sites, randomly generating realistic synthetic precipitation series, and predicting precipitation amounts in excess of those in the observational record.

1. Introduction

Statistical downscaling models are used to estimate weather data at one or more stations based on atmospheric circulation data from a numerical weather prediction model or general circulation model (GCM). Once a model has been developed, downscaled data can be then be entered into an environmental model, for example, a hydrological model for streamflow in a watershed that requires climate information at a finer scale (Xu 1999; Salathe 2005). Historically, most statistical downscaling models have been developed for observations at a single station. If data are required at multiple stations, then a spatial or multisite model is required. Maintaining realistic downscaling relationships between sites is particularly important in hydrological models because streamflow depends strongly on the spatial distribution of precipitation in a watershed. More generally, precipitation is a difficult variable to

downscale because of its nonnormal distribution and its discontinuous behavior in space and time.

Statistical downscaling methods can be placed into three main categories (Wilby and Wigley 1997): (i) regression models, (ii) weather classification schemes, and (iii) weather generators; most multisite precipitation downscaling algorithms falling into the latter two categories, for example, see work by Wilks (1998), Rajagopalan and Lall (1999), Zorita and von Storch (1999), Charles et al. (1999), Buishand and Brandsma (2001), Yates et al. (2003), and Gangopadhyay et al. (2005), among others. Wilks and Wilby (1999) review stochastic weather generators, including a brief discussion of multisite methods and approaches that include a weather classification component.

In practice, all three categories of downscaling models have strengths and weaknesses. In the case of regression, models are tightly linked with the large-scale circulation and, as a result, their application to future climate scenarios from GCMs is straightforward. The goal of this study then is to address some of the shortcomings of the regression-based approach—namely, the poor representation of extreme events, the poor representation of observed variance–covariance, and

Corresponding author address: Alex J. Cannon, Meteorological Service of Canada, 201-401 Burrard St., Vancouver, BC, V6C 3S5, Canada.
E-mail: alex.cannon@ec.gc.ca

the assumption of linearity–normality of data (Wilby et al. 2004)—by introducing a regression model that is fundamentally nonlinear, probabilistic, and targeted on multiple sites. A review of current regression approaches to downscaling is presented to lay the groundwork for the proposed model.

Recent studies have adopted multivariate linear regression models such as canonical correlation analysis or maximum covariance analysis (Uvo et al. 2001) for multisite downscaling tasks. Other methods, such as expanded downscaling (Bürger 1996), extend the multivariate linear regression model by constraining the spatial covariance matrices of the predictions and observations to be the same. Because they are linear in their parameters, these methods may fail when nonlinear relationships are present, for instance, when trying to predict daily precipitation amounts (Yuval and Hsieh 2002). Expanded downscaling deals with nonlinearity by normalizing the predictors and predictands prior to estimating the regression parameters. However, Bürger and Chen (2005) found the resulting model was very sensitive to how the predictors–predictands were normalized. Other forms of nonlinearity—for example, higher-order interactions between predictors—may also be difficult to incorporate into the expanded downscaling model.

Flexible nonlinear regression models like artificial neural networks (ANNs), which can represent arbitrary forms of nonlinearity and complicated interactions between predictors, may yield better predictions than classical linear models for a variable (e.g., precipitation; Yuval and Hsieh 2002). Comparisons between ANNs with multiple outputs versus single outputs have demonstrated the potential of the multivariate approach (Caruana 1997; Mackay 1998), which suggests that multivariate ANNs may be well suited to multisite downscaling. However, trials by the author on a multisite temperature dataset found that model constraints, as in the expanded downscaling model, were needed to ensure that spatial relationships were modeled realistically.

The extension of multivariate ANNs to precipitation, which can be decomposed into separate variables for precipitation occurrence and wet-day amounts, is also not straightforward. Schoof and Pryor (2001) found that ANN downscaling models for the conditional mean of precipitation at a site performed poorly when dry days were modeled at the same time as wet days. Separate models for precipitation occurrence and wet-day amounts are often built for this reason. However, this two-step approach may be difficult to apply in the context of multisite downscaling because, on a given day, precipitation may only fall at some locations. It is

not immediately obvious how to best combine a multivariate ANN for predicting precipitation occurrence with one for predicting precipitation amounts, especially when constraints on spatial variability are also added to the models.

Regression-based models, whether linear or nonlinear, usually only offer point predictions of the conditional mean, which means that realistic estimates of predictive uncertainty are often not available (Cawley et al. 2007). In addition, the variance of the conditional mean will typically be smaller than the variance of the observed series, due in part to the influence of small-scale phenomena that are not represented in the regression model. Expanded downscaling, statistical “inflation,” or the addition of random noise is thus required for the variance of the predicted series to match that of observations (von Storch 1999; Bürger and Chen 2005). Alternatively, the conditional distribution of precipitation amounts can be specified directly, for example, by modeling the parameters of an appropriate statistical distribution rather than just the conditional mean. Williams (1998) successfully described seasonal variations in precipitation using an ANN to model parameters of a mixed Bernoulli–gamma distribution. Haylock et al. (2006) used the same model formulation to downscale precipitation at single sites in the United Kingdom. Recently, Dunn (2004) proposed the Poisson–gamma distribution for similar purposes. The Bernoulli–gamma and Poisson–gamma distributions can be fit to precipitation series that include both dry and wet days. This means that precipitation occurrence and wet-day precipitation amounts can be specified by the same model. To date, this approach has not been extended to multisite downscaling.

As an alternative to purely regression-based models, multisite downscaling models for precipitation have also adopted hybrid approaches whereby a regression model is used as a preprocessor to a nonparametric weather generator, for example, the conditional resampling models of Rajagopalan and Lall (1999) and Buisson and Brandsma (2001), among others. Hybrid methods—for example, Wilby et al. (2003) and Stahl et al. (2008)—are capable of preserving spatial relationships between sites; providing realistic estimates of precipitation occurrence and amounts, including variability; and reproducing the nonnormal distribution of precipitation amounts. Unlike pure regression models, hybrid approaches cannot, as a result of the resampling step, predict daily precipitation amounts in excess of the maximum observed in the historical record. This is true of other nonparametric weather generator or analog downscaling models, although heuristics have been introduced for extrapolating beyond the range of ob-

servations in future climate scenarios (Imbert and Benestad 2005).

The aim of this paper is the development of a regression-based multisite downscaling algorithm for precipitation, the expanded Bernoulli–gamma density network (EBDN), that combines the strengths of the algorithms noted above. Specifically, EBDN can specify the conditional distribution of precipitation at each site, model the occurrence and amount of precipitation simultaneously, reproduce observed spatial relationships between sites, be used as a conditional weather generator to generate synthetic precipitation series, and set new record precipitation amounts. To accomplish these goals, EBDN extends the expanded downscaling model of Bürger (1996) by adopting the ANN-based conditional density estimation approach in conjunction with the Bernoulli–gamma distribution (Williams 1998).

The remainder of the paper is split into five sections. First, data and a benchmark conditional resampling model are described in section 2. The expanded downscaling and the Bernoulli–gamma distribution are reviewed in section 3. The EBDN downscaling model is then introduced in section 4. EBDN is applied to multisite precipitation data, and its results are compared against the benchmark model in section 5. Finally, results are discussed in section 6 along with general conclusions and recommendations for future research.

2. Datasets and benchmarks

a. Precipitation data

Daily precipitation data from 10 climate observing stations along the south coast of British Columbia, Canada, were used to test the EBDN downscaling algorithm. Data from 1959–98 were obtained from the Adjusted Historical Canadian Climate Data archive maintained by the Meteorological Service of Canada (Mekis and Hogg 1999). Station names are given in Table 1, and station locations are shown in Fig. 1.

Southern British Columbia is an area of complex terrain that includes coastal influences and a series of north–south-oriented mountain–valley systems that extend into the interior of the province. The interaction of complex terrain with synoptic-scale storms in the cool, wet season and the influence of convective activity in the warm, dry season gives rise to large spatial gradients in seasonal and annual mean precipitation and high spatial variability on a daily time scale. Correlations between precipitation series over the period range from 0.29 between Estevan Point and Victoria International airports to 0.89 between Estevan Point and Tofino airports.

TABLE 1. Precipitation observing stations.

Station identifier	Station name	Lat	Lon	Elev (m)
C1	Victoria International Airport	48.65	–123.43	20
C2	Comox Airport	49.72	–124.90	24
C3	Port Hardy Airport	50.68	–127.37	22
C4	Estevan Point	49.38	–126.55	7
C5	Pachena Point	48.72	–125.10	37
C6	Tofino Airport	49.08	–125.78	24
C7	Powell River	49.83	–124.50	52
C8	Agassiz Canada Department of Agriculture (CDA)	49.25	–121.77	15
C9	Seymour Falls	49.43	–122.97	244
C10	Vancouver International Airport	49.20	–123.18	3

b. Synoptic-scale predictor data

Synoptic-scale predictors used in the downscaling models were extracted from daily climate fields obtained from the 40-yr European Centre for Medium-Range Weather Forecasts (ECMWF) Re-Analysis (ERA-40; Brankovic and Molteni 2004). Above mean sea level pressure (MSL), 850-hPa relative humidity (RH850), 850-hPa temperature (T850), 700-hPa relative vorticity (V700), and 500-hPa geopotential height (Z500) fields were selected from the archive. Data defined on a $2.5^\circ \times 2.5^\circ$ grid for a spatial domain spanning 35° – 65° N and 145° – 105° W were compressed via an extended principal component analysis. The areal extent of the study area and the gridpoint locations are shown in Fig. 1. The sine and cosine of the day of year were added as predictors to allow for seasonal changes in predictive relationships.

Initially, models were fitted using principal component scores and cyclical variables. However, the resulting models were found to have suboptimal prediction performance, which is consistent with results from Cannon et al. (2002). Instead, the final set of predictors was selected from the grid point, extended principal component, and cyclical variables using a regression tree targeted on the multisite precipitation series (Faucher et al. 1999; Cannon et al. 2002). The optimum regression tree is shown in Fig. 2. Of the original set of predictors, only gridpoint variables from MSL, T850, and RH850 fields appeared in the decision rules. The first split, on MSL at grid point 58 (57.5° N and 130° W), was responsible for more than 60% of the regression tree's reduction in error. This split marks the position and intensity of the frontal systems crossing the coast, with splits down the tree further refining the discrimination between wet and dry events.

In summary, the final set of 10 model predictors included MSL at grid points 45, 58, 114, 127, and 130;

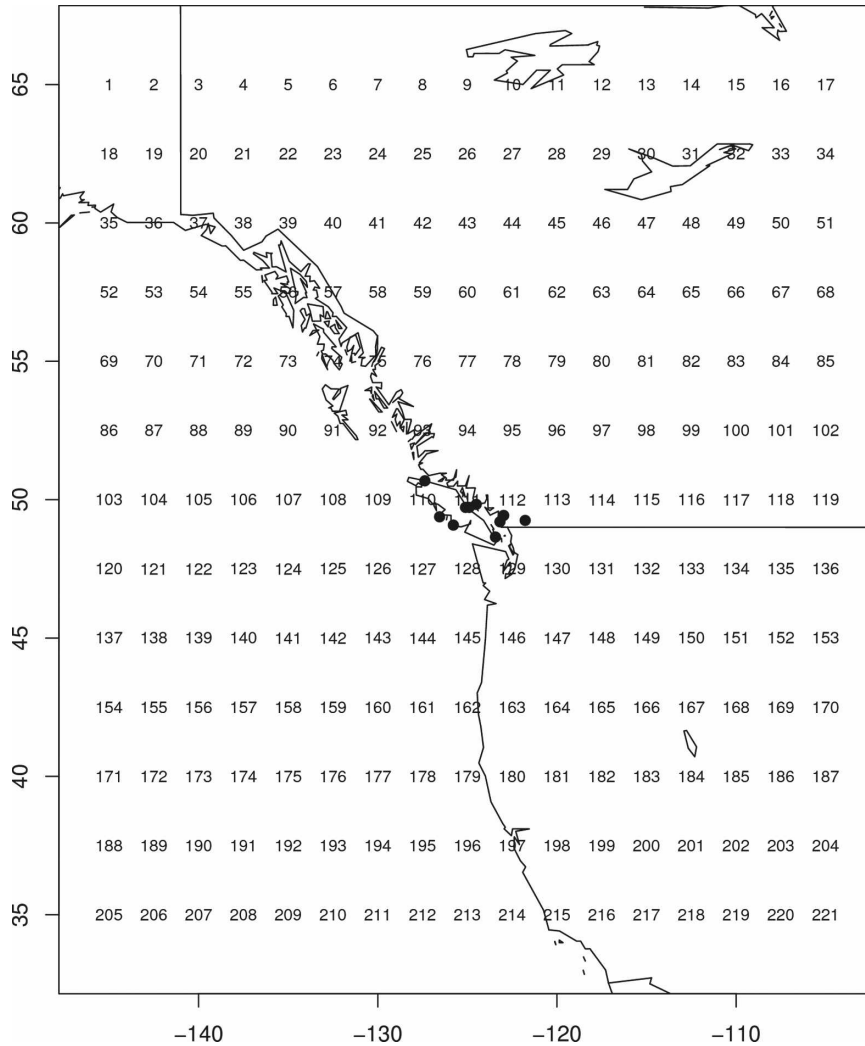


FIG. 1. Map showing the extent of the ERA-40 domain used in the study. Grid points are numbered and filled circles show locations of the precipitation stations.

RH850 at grid points 86 and 99; and T850 at grid points 49, 61, and 86.

c. Benchmark model

The TreeGen downscaling model from Stahl et al. (2008) is used as a benchmark for comparison with the EBDN. TreeGen is hybrid regression–nonparametric weather generator model that generates multisite weather series by conditionally resampling historical observations (Buishand and Brandsma 2001) from synoptic weather types identified via the regression-tree weather-typing algorithm of Cannon et al. (2002). The algorithm, like the proposed EBDN model, is both nonlinear and probabilistic.

For consistency, predictors from section 2b are used as inputs for the TreeGen model. The tree struc-

ture shown in Fig. 2 thus defines the synoptic weather types used in the conditional resampling phase of TreeGen. Once the synoptic map types have been defined from the historical record, predictor fields are entered into the regression tree and each day is assigned to one of the map types. Next, precipitation amounts on a given day are predicted using a nonparametric weather generator based on conditional resampling from cases assigned to that day’s map type (Buishand and Brandsma 2001). The probability $p_T(i)$ of randomly selecting precipitation amounts observed on day i as the predicted values on day t is taken to be inversely proportional to the Euclidean distance $d(t - 1, i - 1)$ between the predicted values on the previous day $t - 1$ and historical values of the precipitation amounts on day $i - 1$,

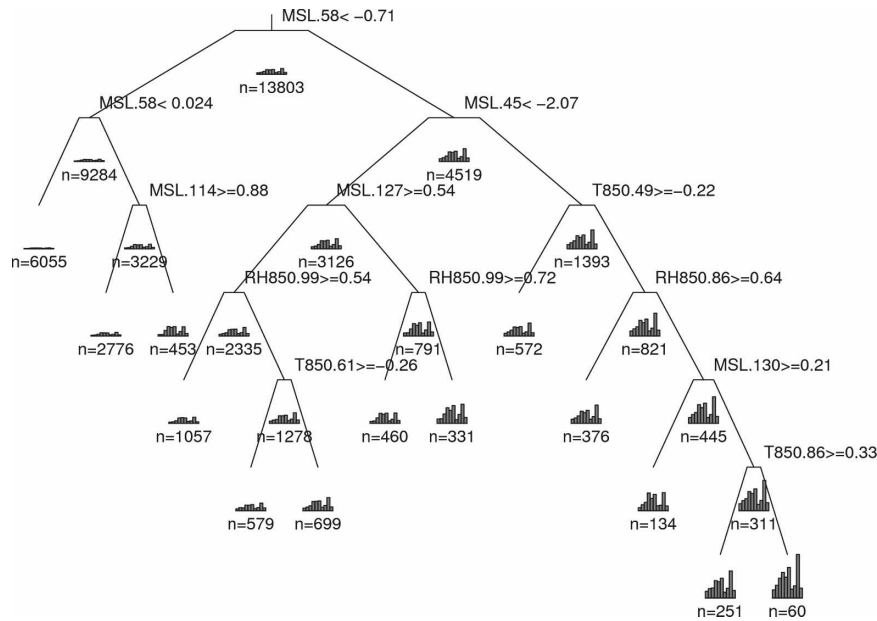


FIG. 2. Multivariate regression tree used for predictor selection in the EBDN model. Splits in the tree are labeled by meteorological field and gridpoint number from Fig. 1. At each node in the tree, bar plots show the relative magnitude of mean precipitation amounts at the 10 stations.

$$p_T(i) = \frac{[d(t-1, i-1) + 0.1]^{-2}}{\sum_{h \in H} [d(t-1, h-1) + 0.1]^{-2}}, \quad (1)$$

where H is the set of historical days assigned to the predicted map type occurring on day t .

3. Background

a. Expanded downscaling

The probabilistic multisite precipitation downscaling method developed in the current study extends the deterministic expanded downscaling model of Bürger (1996, 2002). Expanded downscaling is based on the multivariate linear regression model. Given an $N \times I$ matrix of predictors \mathbf{X} , where $x_i(t)$ is the value of the i th predictor ($i = 1, \dots, I$) at time t ($t = 1, \dots, N$) and a corresponding $N \times M$ matrix of predictands \mathbf{Y} , where $y_m(t)$ is the value of the m th predictand and ($m = 1, \dots, M$) at time t , predictions $\hat{\mathbf{Y}}$ from the standard multivariate linear regression model are given by

$$\hat{\mathbf{Y}} = \mathbf{X}\mathbf{W}, \quad (2)$$

where \mathbf{W} is the matrix of regression parameters. The least squares error solution to the multivariate linear regression model is given by

$$\mathbf{W} = (\mathbf{X}^T\mathbf{X})^{-1}\mathbf{X}^T\mathbf{Y}. \quad (3)$$

Intercept terms can be incorporated by adding a unit column vector to \mathbf{X} .

In expanded downscaling, elements of \mathbf{W} are instead found by minimizing the least squares error subject to the added constraint

$$\hat{\mathbf{S}}_{\hat{\mathbf{Y}}} = \mathbf{W}^T \mathbf{S}_{\mathbf{X}} \mathbf{W} = \mathbf{S}_{\mathbf{Y}}, \quad (4)$$

where $\mathbf{S}_{\hat{\mathbf{Y}}}$ is the covariance matrix of $\hat{\mathbf{Y}}$,

$$\hat{\mathbf{S}}_{\hat{\mathbf{Y}}} = \frac{\hat{\mathbf{Y}}_c^T \hat{\mathbf{Y}}_c}{N}, \quad (5)$$

and $\hat{\mathbf{Y}}_c$ is the matrix of predictions with columns centered to zero mean; similarly, $\mathbf{S}_{\mathbf{X}}$ is the covariance matrix of the observed predictors \mathbf{X} , and $\mathbf{S}_{\mathbf{Y}}$ is the covariance matrix of the observed predictands \mathbf{Y} .

b. Bernoulli–gamma distribution

To move expanded downscaling from a deterministic modeling framework to a probabilistic modeling framework, an appropriate probability density function (pdf) must be selected to represent the distribution of precipitation at the observing sites. Williams (1998) suggested using a mixed Bernoulli–gamma distribution for describing precipitation series that include both days with no precipitation and days with precipitation. This mixed distribution was used in single site precipitation

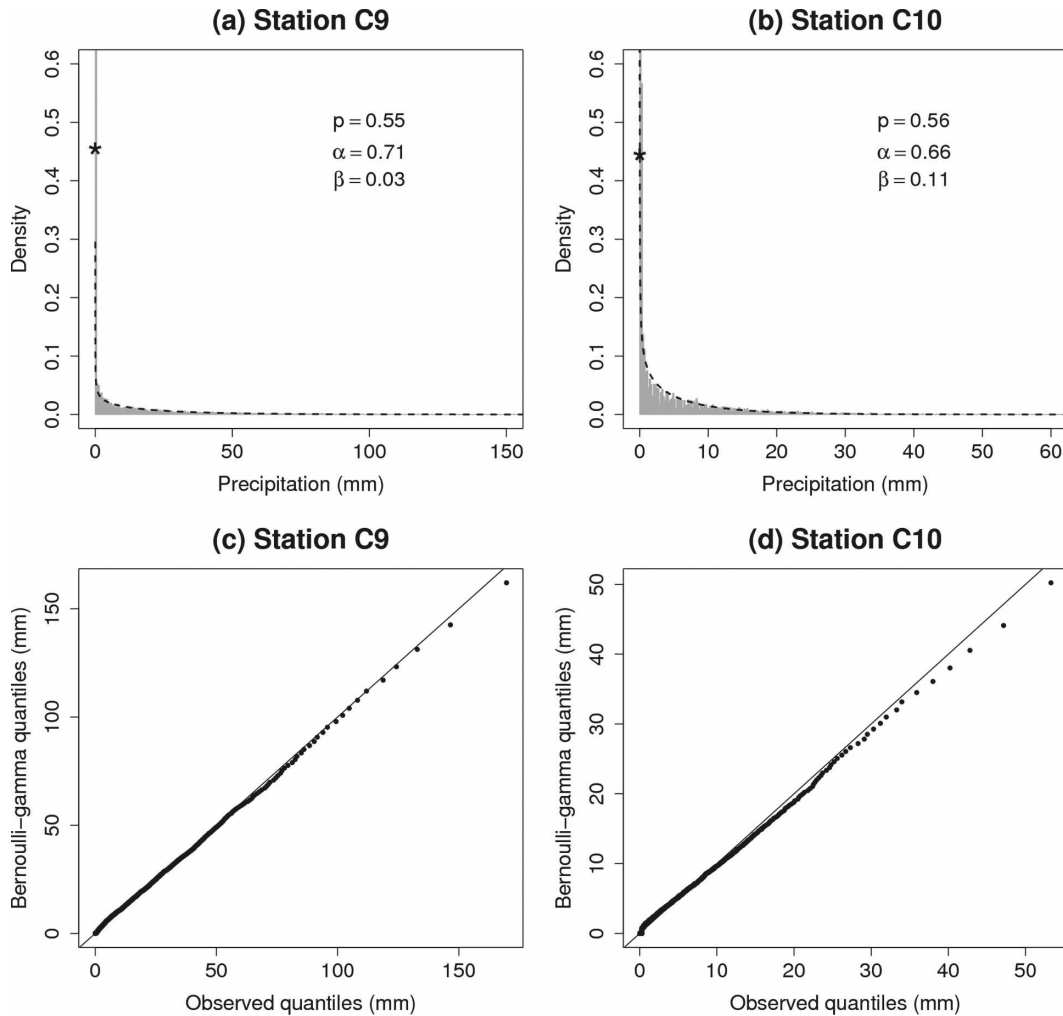


FIG. 3. Histograms of observed precipitation (gray shading) and fitted Bernoulli-gamma pdfs (dashed line for positive amounts and asterisk for the probability at zero) at (a) station C9 and (b) station C10, along with quantile-quantile plots for (c) station C9 and (d) station C10.

downscaling models by Haylock et al. (2006) and Cawley et al. (2007).

The Bernoulli-gamma pdf is given by

$$f(y; p, \alpha, \beta) = \begin{cases} 1 - p & \text{for } y = 0 \\ \frac{p(y/\beta)^{\alpha-1} \exp(-y/\beta)}{\beta\Gamma(\alpha)} & \text{for } y > 0 \end{cases}, \quad (6)$$

where y is the precipitation amount, p ($0 \leq p \leq 1$) is the probability of precipitation, α ($\alpha > 0$) is the shape parameter of the gamma distribution, β ($\beta > 0$) is the scale parameter of the gamma distribution, and $\Gamma(\cdot)$ is the gamma function. The mean value of the distribution is $\mu^{(B)} = p\alpha\beta$, and the variance is $s^{(B)} = p\alpha[1 + (1-p)\alpha]\beta^2$.

To illustrate, a Bernoulli-gamma distribution was fit to observations at station C9, the highest elevation site

with the largest mean annual precipitation of the 10 stations, and station C10, the lowest elevation site receiving approximately one-third the precipitation of station C9. Values of p were estimated directly from the observations, whereas α and β were set via the method of maximum likelihood. Histograms of the observed series and the fitted Bernoulli-gamma pdfs, in addition to quantile-quantile plots, are shown in Fig. 3. The Bernoulli-gamma distribution fit the observed data well at both stations, although the highest quantiles at station C10 were underpredicted slightly.

4. Method

a. Bernoulli-gamma density network

The EBDN downscaling methodology extends expanded downscaling by (i) using an ANN for the

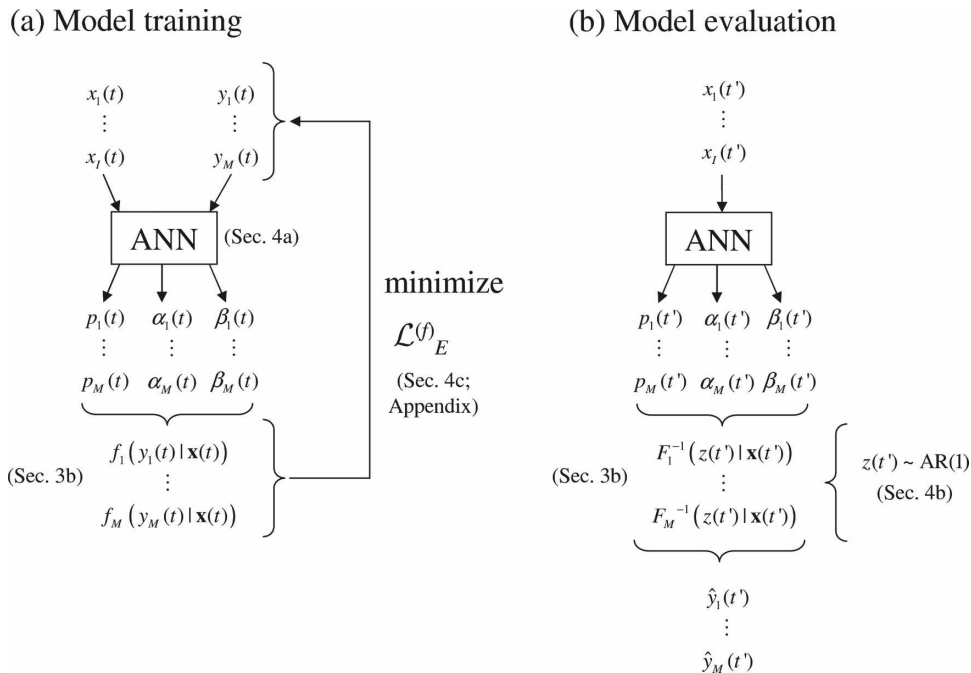


FIG. 4. Flowchart showing the steps involved in (a) training and (b) evaluating the EBDN model. Relevant sections of the text are given in parentheses.

predictor–predictand mapping and (ii) using the Bernoulli–gamma distribution to represent the predictive density of precipitation at multiple observing sites. For reference, Fig. 4 shows the steps involved in training and evaluating outputs from the model given new data. The first step is to train the ANN.

In most applications, ANNs are trained to minimize a least squares cost function. The resulting model describes a mapping that approximates the conditional mean of the prediction and data. This mapping is optimal if the data are generated from a deterministic function that is corrupted by a normally distributed noise process with constant variance (Bishop 1995, section 6.1–6.2). When the noise process has nonconstant variance or is nonnormal then a more general model—one that fully describes the conditional density of the predictand and data rather than just the conditional mean—is more appropriate. This can be accomplished by adopting an ANN with outputs for each parameter in the pdf of the assumed noise process. A conditional density ANN for a normally distributed noise process with nonconstant variance would thus have two outputs: one for the conditional mean and one for the conditional variance Dorling et al. (2003). For the Bernoulli–gamma density network (BDN), three outputs, one for each parameter in the distribution, are required.

The architecture of the BDN is shown schematically

in Fig. 5. In this example, the model has $K = 6$ outputs, corresponding to the three Bernoulli–gamma parameters (p , α , and β) at $M = 2$ sites. The number of model outputs for an arbitrary number of observing sites is $3M$.

Given predictors x_i ($i = 1, \dots, I$) for the observed precipitation series y_m ($m = 1, \dots, M$), results from the BDN are evaluated in the same manner as a standard ANN. First, output from the j th hidden-layer node h_j is given by applying the hyperbolic tangent function to the inner product between the predictors x_i and the input-hidden layer weights $w_{j,i}^{(1)}$ plus the bias $b_j^{(1)}$:

$$h_j(t) = \tanh \left[\sum_{i=1}^I x_i(t) w_{j,i}^{(1)} + b_j^{(1)} \right]. \quad (7)$$

The predicted value of the k th output from the network o_k is then given by

$$o_k(t) = \sum_{j=1}^J h_j(t) w_{k,j}^{(2)} + b_k^{(2)}, \quad (8)$$

where $w_{k,j}^{(2)}$ are the hidden-output layer weights and $b_k^{(2)}$ are the hidden-output layer biases. $g_k[\cdot]$ are functions that constrain the outputs to lie within the allowable ranges of the Bernoulli–gamma distribution parameters. For the first site ($m = 1, k = 1, \dots, 3$), this leads to

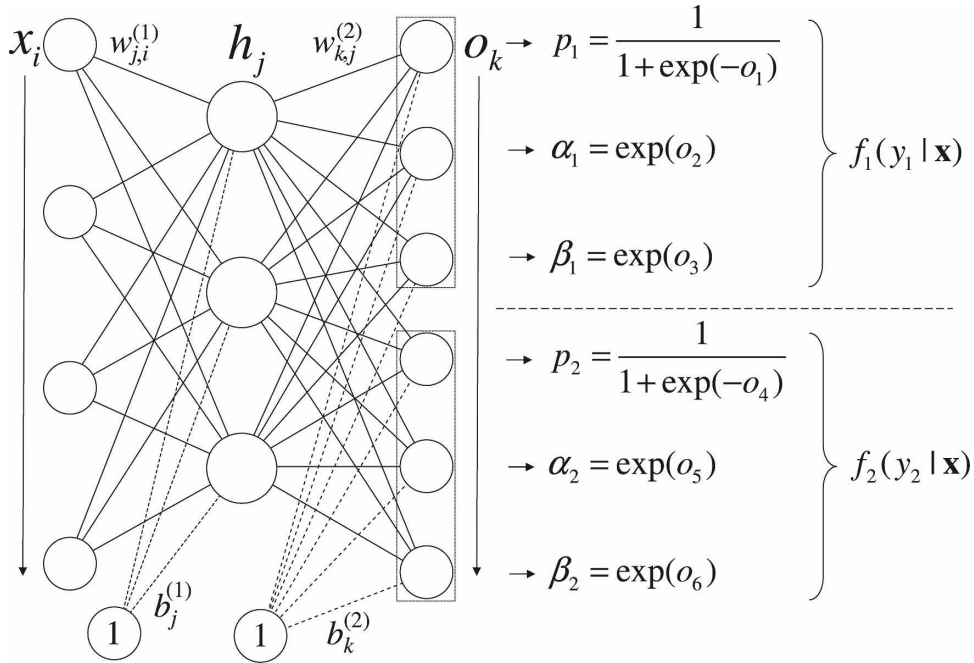


FIG. 5. Sample schematic diagram of a Bernoulli–gamma density ANN for modeling conditional Bernoulli–gamma distribution parameters at two sites.

$$p_1(t) = g_1[o_1(t)] = \frac{1}{1 + \exp[-o_1(t)]}, \quad (9)$$

$$\alpha_1(t) = g_2[o_2(t)] = \exp[o_2(t)], \quad (10)$$

$$\beta_1(t) = g_3[o_3(t)] = \exp[o_3(t)], \quad (11)$$

and so on for the remaining $M - 1$ sites. The conditional Bernoulli–gamma pdf at time t and at site m , $f_m[y_m(t)|x(t)]$, is then given by Eq. (6) with the parameters $p_m(t)$, $\alpha_m(t)$, and $\beta_m(t)$.

Because the BDN gives probabilistic outputs, weights and biases in the model are set following the method of maximum likelihood by minimizing the negative log predictive density (NLPD) cost function (Williams 1998; Haylock et al. 2006; Cawley et al. 2007)

$$\mathcal{L} = - \sum_{t=1}^N \sum_{m=1}^M \log\{f_m[(y_m(t)|x(t))]\}, \quad (12)$$

via a quasi-Newton minimization algorithm (Schnabel et al. 1985).

As is the case with a conventional ANN, the overall complexity of the model should be limited to ensure that the model generalizes well to new data. Standard methods for controlling model complexity—for example, choosing the number of hidden nodes via cross-validation (Dimopoulos et al. 1999), Bayesian regularization (Williams 1998; Cawley et al. 2007), ensemble

averaging (Cannon and Whitfield 2002), early stopping (Gardner and Dorling 1998), or other algorithms—should thus be used to ensure that the BDN does not overfit the training dataset.

b. Conditional simulation of precipitation series

Once a BDN has been trained, it can be used to create synthetic time series of precipitation amounts \hat{y}_m by randomly generating a series of cumulative probabilities z from a uniform distribution and then evaluating quantiles from an inverse Bernoulli–gamma conditional distribution function (cdf), $F_m^{-1}(z)$, with parameters given by the BDN. This approach was taken by Cawley et al. (2007). However, as shown by Huth et al. (2001), the time structure of the downscaled series may be poorly simulated if z is generated by a white noise process.

Following Bürger and Chen (2005), the series z is instead assumed to be first-order autoregressive AR(1), which means that it can be randomly generated by first creating an autocorrelated series with zero mean and unit variance

$$u(t) = u(t - 1)\tau + \epsilon(t)(1 - \tau^2)^{1/2}, \quad (13)$$

where τ is the lag-1 autocorrelation of the series to be generated and $\epsilon \sim \mathcal{N}(0, 1)$. The series u is then trans-

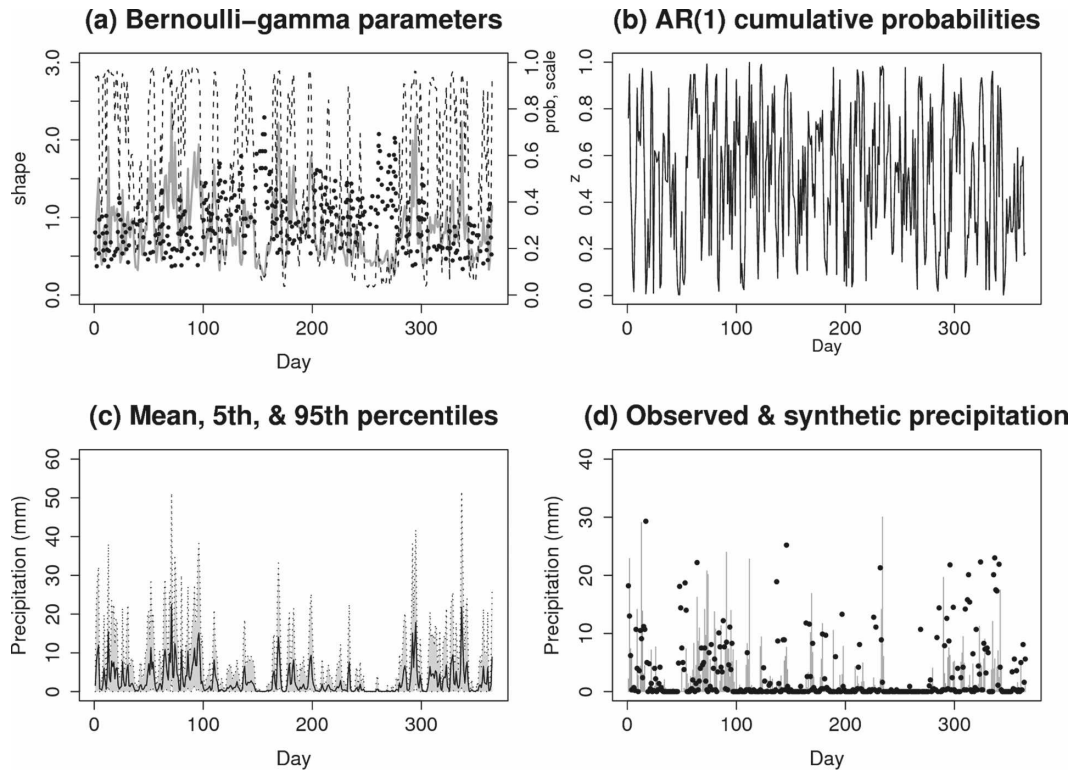


FIG. 6. Results shown for station C10 during 1989. Time series of (a) conditional Bernoulli–gamma parameters, where the probability of precipitation $p(t)$ is shown by the dashed line, the shape $\alpha(t)$ by the gray solid line, and the scale $\beta(t)$ by the dotted line; (b) AR(1) cumulative probabilities $z(t)$; (c) conditional mean (solid line) and the range from the conditional 5th to 95th percentiles (gray shading); and (d) synthetic precipitation obtained by combining (a) and (b) (vertical gray lines) and observed precipitation values (dots).

formed by the standard normal cdf, $\Phi[\cdot]$, so that it lies in the range $[0, 1]$,

$$z(t) = \Phi[u(t)]. \quad (14)$$

The AR(1) model is chosen for its parsimony. In practice, more complicated noise models could be applied instead.

At time t , the value of the synthetic precipitation time series $\hat{y}_m(t)$ is given by $F_m^{-1}[z(t)]$ with parameters $p_m(t)$, $\alpha_m(t)$, and $\beta_m(t)$. The value of τ is chosen via trial and error such that the lag-1 autocorrelations of the generated series and observed series match as closely as possible. To illustrate this process, sample results from a BDN model with five hidden-layer nodes are shown in Fig. 6 for station C10 during 1998. Each panel, moving from the conditional Bernoulli–gamma parameters through to the estimation of the synthetic series, corresponds to a step in the flowchart shown in Fig. 4b.

c. Expanded Bernoulli–gamma density network

Following expanded downscaling, the EBDN extends the BDN model by adding a constraint on the

simulated covariance matrix to the model cost function. Direct translation of Eq. (4), the constrained least squares cost function from expanded downscaling, to the probabilistic framework of the EBDN leads to the following cost function:

$$\begin{aligned} \mathcal{L}_E = & - \sum_{t=1}^N \sum_{m=1}^M \log\{f_m[y_m(t)|x(t)]\} \\ & + \gamma \sum_{m=1}^M \sum_{q=m}^M (s_{y_{m,q}} - s_{\hat{y}_{m,q}})^2, \end{aligned} \quad (15)$$

where the first term is the NLPD summed over the M sites, and the second term is the sum of squared differences between elements of the covariance matrix \mathbf{S}_Y for pairs of observed series y_m and the corresponding elements of the covariance matrix $\mathbf{S}_{\hat{Y}}$ for pairs of predicted series \hat{y}_m . The coefficient γ controls the relative scaling of the NLPD and the constraint on the covariances.

Unfortunately, the evaluation of \mathcal{L}_E is computationally intensive and its minimization is impractical because synthetic series \hat{y}_m must be generated to estimate the predicted covariance matrix $\mathbf{S}_{\hat{Y}}$. Instead, a strategy

TABLE 2. Cross-validated model performance statistics for EBDN and TreeGen downscaling models with the true skill statistic (TSS), hit-rate (HIT), probability of detection (POD), false alarm rate (FAR), and bias ratio (BIAS) for binary predictions of precipitation occurrence. Values corresponding to the better-performing model are italicized. *rmse* and *r_s* indicate the root mean squared error and correlation coefficient between observed values and the predicted conditional mean. The subscript *s* refers to values calculated for the spatial mean over the 10 stations.

Statistic	EBDN	TreeGen
NLPD	<i>2.4</i>	∞ (3.8)
<i>rmse</i> (mm)	<i>11.7</i>	11.9
<i>rmse_s</i> (mm)	<i>7.4</i>	8.1
<i>r_s</i>	<i>0.63</i>	0.53
TSS	<i>0.52</i>	0.39
HIT	<i>0.77</i>	0.68
POD	<i>0.69</i>	<i>0.77</i>
FAR	<i>0.26</i>	0.40
BIAS	<i>0.93</i>	1.29

for reducing the computational cost, which is presented in the Appendix, is used throughout the remainder of the paper.

5. Results

Precipitation data from 10 stations along the south coast of British Columbia were regressed, using the EBDN model, onto the 10 synoptic-scale predictors selected in section 2. Models were evaluated using cross-validation. Data were split into four decade-long segments (1959–68, 1969–78, 1979–88, and 1989–98), models were trained on three of the four segments, and predictions were then made on the held-out segment. Model training followed the procedure outlined in the appendix. This procedure was repeated, each time rotating the held-out segment, until predictions had been made on all the data. A secondary fivefold cross-validation was conducted on the training segments to determine the optimal number of hidden nodes in the EBDN, that is, to avoid model overfitting. Five hidden nodes were selected by consensus. Following cross-validation, predictions on the test segments were concatenated and validated against observations.

Statistics measuring probabilistic, deterministic, and categorical performance of the EBDN and TreeGen models are given in Table 2. In terms of probabilistic performance, the mean NLPD over all stations and days was 2.4 for the EBDN model and ∞ for the TreeGen model. Because TreeGen is based on a nonparametric weather generator, it cannot generate precipitation amounts in excess of those in the training dataset (i.e., the predicted pdf has a finite upper bound equal to the maximum observed precipitation). Thus, predicted probability densities are zero, with a corresponding NLPD of ∞ , whenever precipitation amounts are out-

side the range of the training data. When out of range values were removed from cross-validation test segments, the NLPD fell to 3.8 for TreeGen and to 2.3 for EBDN. For reference, unconditional Bernoulli–gamma distributions were also fit to observed series at each station. The resulting climatological NLPD was 2.6. Results are consistent with those reported by Cawley et al. (2006) for a single-site precipitation downscaling task, wherein a small improvement in NLPD relative to climatology was noted for a Bernoulli–gamma density network.

Although both the EBDN and TreeGen models give probabilistic predictions, point forecasts can also be made by estimating the conditional mean of the pdf on each day. Values of the root-mean-square error (*rmse*) and the Pearson product-moment correlation based on deterministic predictions are shown in Table 2. Values of *rmse* for the two models were within 0.2 mm of one another and are consistent with those found by Cannon (2007b) using a coupled ANN–analog downscaling model. The EBDN model predicted the spatial mean more accurately than TreeGen, showing a 10% improvement in *rmse_s*, and values of *r_s* corresponding to 40% explained variance versus 28% for TreeGen.

Conditional probabilities of precipitation occurrence were calculated from the conditional EBDN and TreeGen pdfs with cumulative probabilities exceeding 0.5, resulting in a prediction of measurable precipitation. Categorical measures of performance were then calculated based on the 2×2 contingency table (Wilks 2006). Again, results are given in Table 2. Based on the true skill statistic, both models showed positive skill relative to climatology, although EBDN outperformed TreeGen. Although TreeGen exhibited a slightly higher probability of detection, this was offset by EBDN having fewer false alarms, a higher hit rate, and a bias ratio closer to one.

To evaluate multisite performance and the ability of the constrained cost function to replicate the observed covariance matrix, 100 realizations of the synthetic series \hat{y}_m at the 10 sites were generated following section 4b. Observed and predicted covariances between sites are plotted in Fig. 7 for the EBDN and TreeGen models. In all cases, the distribution of the EBDN covariances across the 100 realizations overlapped observed values, whereas the magnitude of TreeGen covariances tended to be lower than observed, particularly for the highest magnitudes. As a further check on the ability of the models to simulate spatially realistic precipitation fields, quantile–quantile plots for observed and predicted daily average precipitation over the 10 stations are shown in Fig. 8. Results indicate that the distribution of the spatial average series from the EBDN model

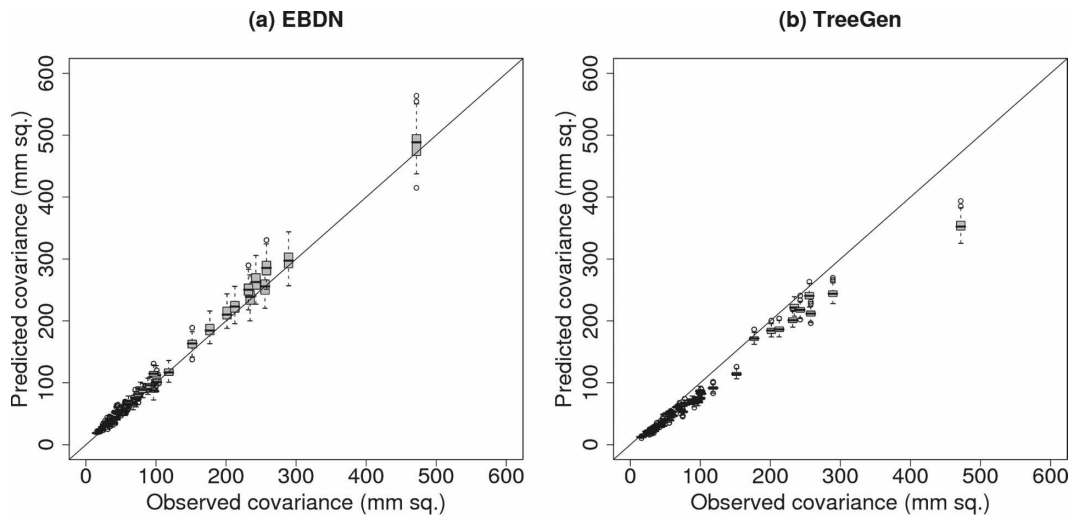


FIG. 7. Observed covariances vs boxplots of predicted covariances from 100 synthetic precipitation series from (a) the EBDN model and (b) the TreeGen model. The line inside each box represents the median, boxes extend from the 25th to 75th percentiles, whiskers extend to points within 1.5 times the interquartile range, and outliers are shown as circles.

matched observations, whereas quantiles were slightly underpredicted by TreeGen.

To assess the EBDN model's ability to replicate observed precipitation variability on a seasonal and inter-annual basis, Figs. 9 and 10 show monthly distributions of four statistics: (i) the number of wet days (NWD), (ii) maximum five-day precipitation amounts (PX5D), (iii) maximum number of consecutive wet days (WRUN), and (iv) maximum number of consecutive dry days (DRUN). Two stations, C4, which is located near sea level on the west coast of Vancouver Island, and C9, which is the highest elevation station on the mainland, were selected to represent different climatic

regions within the study domain. The degree of correspondence between the observed and modeled values during the year are summarized in Table 3, which lists rmse values for the median range and interquartile range (IQR) of the distributions shown in Figs. 9 and 10. In general, the EBDN model performed better than TreeGen, although both models were able to reproduce seasonal variations in precipitation characteristics at the two sites. EBDN had lower rmse values than TreeGen for the median for all four statistics at both stations. Interannual variability, when measured by the interquartile range, was better reproduced by EBDN for NWD and DRUN at station C4 but only for DRUN at

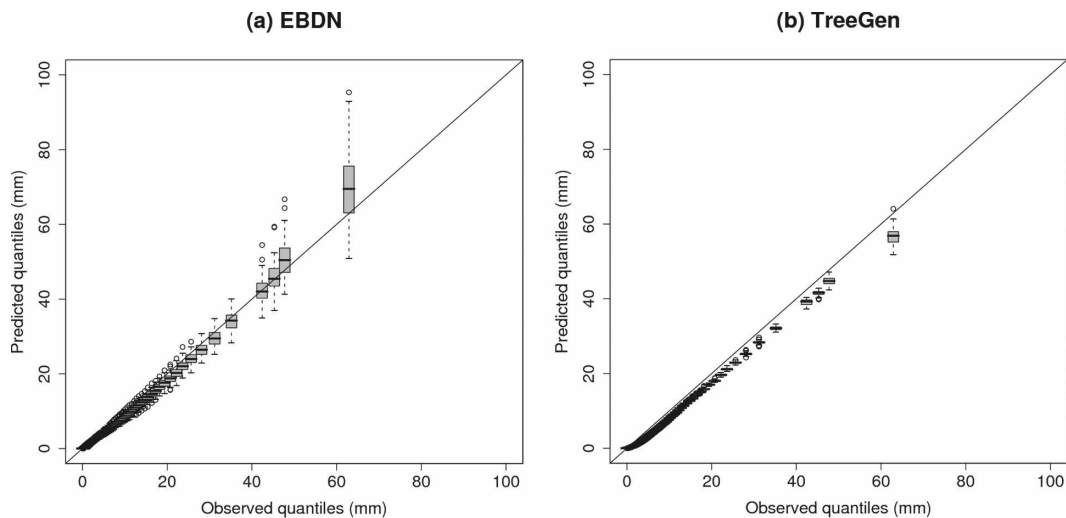


FIG. 8. Quantile-quantile plots of station mean precipitation based on 100 synthetic precipitation series from the (a) EBDN and (b) TreeGen models.

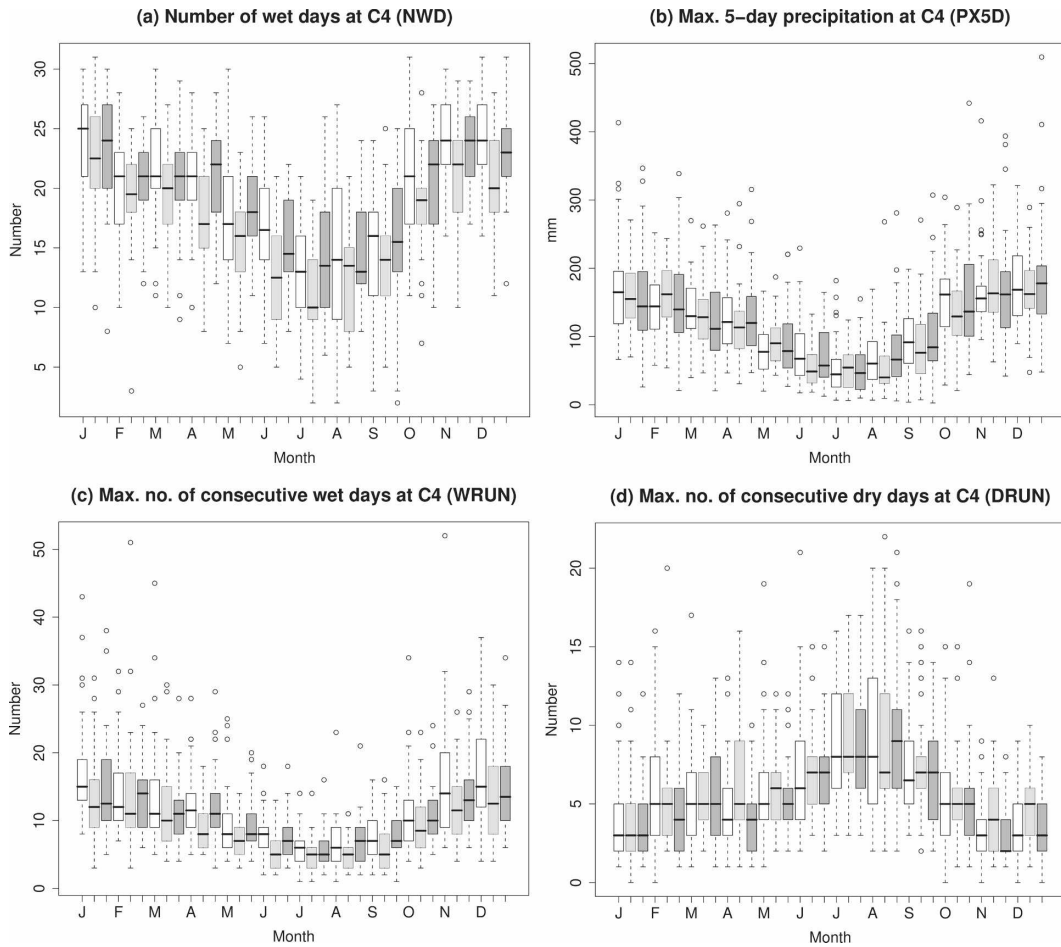


FIG. 9. Interannual distributions of monthly observed (white boxes), TreeGen modeled (light gray boxes), and EBDN modeled (dark gray boxes) showing (a) NWD, (b) PX5D, (c) WRUN, and (d) DRUN at station C4. Boxplots are constructed as described in Fig. 7.

station C9. Eleven of the 16 statistics were better simulated by EBDN than by TreeGen. It bears noting that these results were from a single synthetic realization from both the EBDN and TreeGen models. As a result, they do not capture the variability due to the stochastic nature of the two algorithms. That being said, results from multiple runs were inspected, and the general patterns seen in Figs. 9 and 10 and Table 3 were also found in the additional model runs.

6. Discussion and conclusions

This study introduced a probabilistic synoptic downscaling model for precipitation at multiple sites. The EBDN model modifies the expanded downscaling model of Bürger (1996, 2002) by adopting an ANN model that predicts parameters of the Bernoulli-gamma distribution rather than point precipitation values. This extends the density network approach of Wil-

liams (1998) and Haylock et al. (2006) from single site to multisite datasets. Weights and biases in the ANN model are found by minimizing a constrained NLPD cost function. The constraint on predicted covariances from expanded downscaling is split into separate terms for the site variances and the intersite correlations in the EBDN model. This reduces the number of computations required to evaluate the cost function by allowing predicted series of Bernoulli-gamma parameters to replace stochastically generated precipitation series in calculations of the constraint terms.

The verification of historical precipitation data from 10 sites on the south coast of British Columbia suggests that the EBDN model may be a useful tool for generating multisite climate scenarios based on synoptic-scale climate data from GCMs. The EBDN model performed better than a benchmark hybrid regression-weather generator model on most verification statistics. Although the improvement in NLPD between the

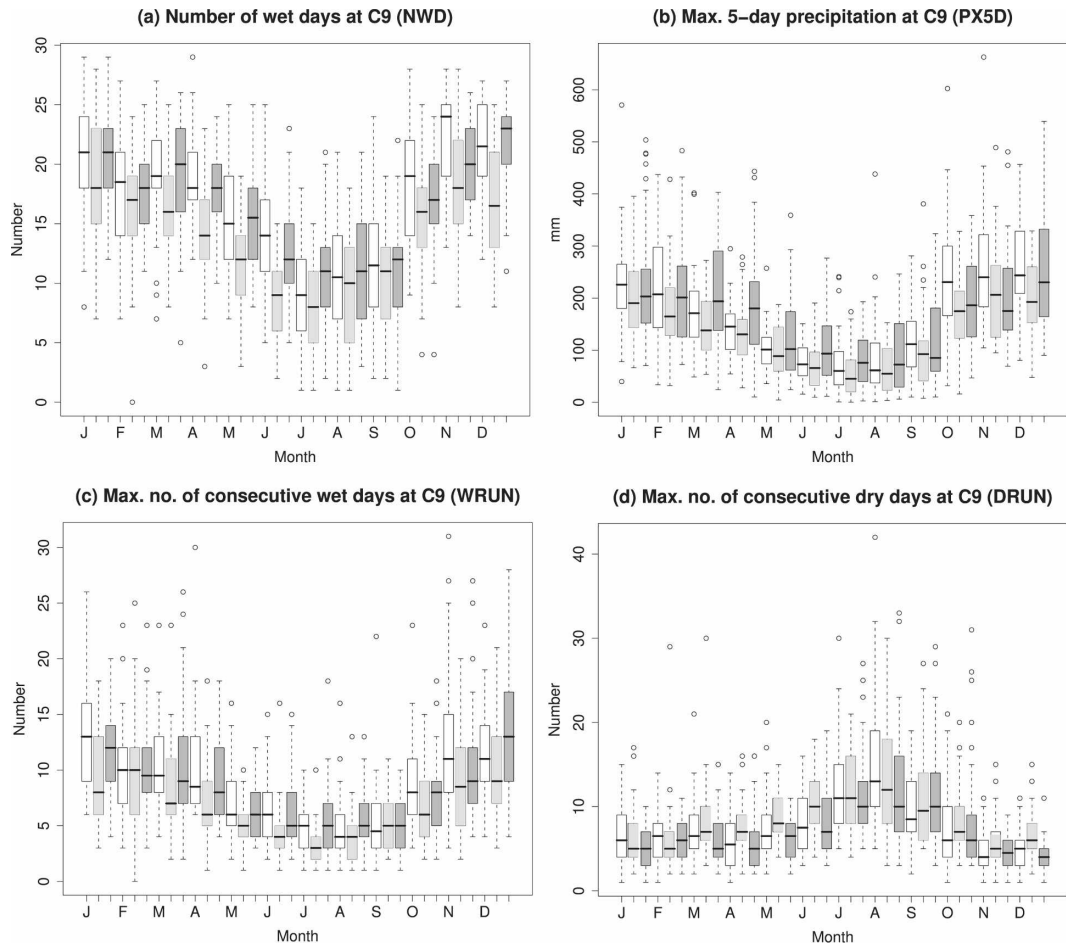


FIG. 10. Same as Fig. 9, but for station C9.

EBDN model and the climatological distribution was small, model evaluations suggest that the EBDN model is capable of generating a series with realistic spatial and temporal variability. A more rigorous analysis of the model's ability to reproduce weekly, monthly, seasonal, and annual variability, along with observed trends, is currently underway as part of a larger project

testing a suite of multisite precipitation downscaling methods, including analog and weather-typing models. It is worth noting that the EBDN model—unlike analog or weather-typing models—does not require any heuristics to extrapolate beyond the range of the training observations (Imbert and Benestad 2005).

Temporally, constraints on the covariance matrix,

TABLE 3. Cross-validated model rmse statistics for median range and IQR of monthly NWD, PX5D, WRUN, and DRUN for EBDN and TreeGen downscaling models at stations C4 and C9. Results summarize Figs. 9 and 10. Values corresponding to the better-performing model are italicized.

Station	Variable	Unit	RMSE median		RMSE IQR	
			EBDN	TreeGen	EBDN	TreeGen
C4	NWD	(days)	<i>0.93</i>	2.58	<i>1.73</i>	2.16
C4	PX5D	(millimeters)	<i>12.0</i>	15.4	<i>19.5</i>	<i>16.6</i>
C4	WRUN	(days)	<i>1.18</i>	2.12	<i>1.85</i>	<i>1.33</i>
C4	DRUN	(days)	<i>0.59</i>	0.88	<i>1.17</i>	1.49
C9	NWD	(days)	<i>1.64</i>	3.44	<i>1.74</i>	<i>1.51</i>
C9	PX5D	(millimeters)	<i>29.0</i>	31.8	<i>38.8</i>	<i>24.6</i>
C9	WRUN	(days)	<i>1.00</i>	2.25	<i>1.24</i>	<i>1.05</i>
C9	DRUN	(days)	<i>1.21</i>	1.27	<i>0.85</i>	1.15

along with the value of τ used in the conditional simulation, are specified using estimates spanning the entire seasonal cycle. Temporal variations could also be incorporated by enforcing seasonal or monthly constraints on the site variances–correlations and by changing τ throughout the year (Schoof and Robeson 2003). Minimal changes to the model would be required to accommodate finer-grained control over the temporal variability.

Although Bürger (2002) applied the expanded downscaling to multisite precipitation data, it was originally proposed as a general method for modeling multiple variables (e.g., precipitation, temperature, wind components, and others) at one or more sites (Bürger 1996). The extension of the EBDN to variables other than precipitation would require that appropriate distributions to be identified and incorporated into the ANN model. Other parametric distributions or mixtures of distributions would, in addition to the pdf and cdf, need expressions for the mean and variance (in terms of the distribution parameters) to be specified to be used within the proposed modeling framework. Work on a more general version of the model is currently underway.

Precipitation in southern British Columbia is characterized by high spatial and temporal variability due in part to the area's complex terrain. Although results for stations in the wet, maritime climate of the south coast are encouraging, more work is needed to validate the EBDN model in other climatic regions. Preliminary results on data from the Kootenay region of British Columbia, which is characterized by a more continental climate, suggest comparable levels of skill to those reported here (Cannon 2007a).

Predictions from the EBDN are probabilistic, which means that any relevant descriptor of the Bernoulli–gamma distribution, including means, variances, quantiles, and posterior probabilities of exceeding a given threshold, can be obtained from the model. As Cawley et al. (2007) demonstrate, estimates of predictive uncertainty from downscaling models can be very useful in impact studies, especially when consequences of extreme events are of key concern. The suitability of the EBDN model for use in generating precipitation data for hydrological models or spatial interpolation algorithms, both of which require spatially realistic input data, should also be assessed. Results suggest that the EBDN model's ability to reproduce spatial relationships between sites, along with its ability to model precipitation extremes, make it well suited for these tasks.

Acknowledgments. This work was supported by the Meteorological Service of Canada while the author was

a member of the Department of Earth and Ocean Sciences at the University of British Columbia.

APPENDIX

Calculating the EBDN Cost Function

From section 4c, the cost function used to train the EBDN model is given by

$$\mathcal{L}_E = -\sum_{t=1}^N \sum_{m=1}^M \log\{f_m[y_m(t)|x(t)]\} + \gamma \sum_{m=1}^M \sum_{q=m}^M (s_{y_{m,q}} - s_{\hat{y}_{m,q}})^2, \quad (\text{A1})$$

where the first term is the NLPD summed over the M sites. The second term is the sum of squared differences between elements of the observed covariance matrix \mathbf{S}_Y and the corresponding elements of the predicted covariance matrix $\mathbf{S}_{\hat{Y}}$, and γ controls the relative weighting of the two terms.

To reduce sampling variability, estimates of $\mathbf{S}_{\hat{Y}}$ should be averaged over values from many realizations of the synthetic series \hat{y}_m , which, as described in section 4b, are generated by randomly drawing serially correlated samples from the Bernoulli–gamma distributions. This can be computationally expensive, which effectively rules out the use of \mathcal{L}_E as the cost function for training the EBDN model.

As an alternative, a modified cost function that allows calculations involving \hat{y}_m to be replaced with calculations involving the Bernoulli–gamma distribution parameters p_m , α_m , and β_m , which are available directly and without further computation as outputs from the ANN, is proposed. One simple option would be to calculate the predicted covariance matrix from the conditional means $\mu_m^{(B)}$ instead of the synthetic series \hat{y}_m . This would, however, force the series of conditional means at each site to have the same variance as the observed series, which would degrade the density estimation, essentially resulting in deterministic predictions similar to those from the original expanded downscaling algorithm of Bürger (1996).

Instead, the modified cost function makes use of the fact that the covariance matrix can be expressed in terms of separate contributions from the site variances and the correlations between sites. When estimating elements of the correlation matrix for the predictions, the synthetic series \hat{y}_m can be replaced with the series of conditional means $\mu_m^{(B)}$. Because correlations are insensitive to the linear rescaling of variables, this replacement will not—as is the case above for the covari-

ances—degrade the probabilistic performance of the model.

To illustrate this process, the covariance matrix for the predictions $\hat{\mathbf{Y}}$ can be decomposed as

$$\mathbf{S}_{\hat{\mathbf{Y}}} = \mathbf{V}_{\hat{\mathbf{Y}}}\mathbf{R}_{\hat{\mathbf{Y}}}\mathbf{V}_{\hat{\mathbf{Y}}}, \quad (\text{A2})$$

where $\mathbf{V}_{\hat{\mathbf{Y}}}$ is a diagonal matrix of standard deviations (i.e., with diagonal elements $s_{\hat{y}_m}^{1/2}$, and $\mathbf{R}_{\hat{\mathbf{Y}}}$ is the correlation matrix)

$$\mathbf{R}_{\hat{\mathbf{Y}}} = \frac{\hat{\mathbf{Y}}_s^T \hat{\mathbf{Y}}_s}{N}, \quad (\text{A3})$$

with $\hat{\mathbf{Y}}_s$ the matrix of predictions with columns centered to zero mean and scaled to unit variance. The cost function now becomes

$$\begin{aligned} \mathcal{L}'_E = & -\sum_{t=1}^N \sum_{m=1}^M \log\{f_m[y_m(t)|x(t)]\} + \gamma_1 \sum_{m=1}^M (s_{y_m} - s_{\hat{y}_m})^2 \\ & + \gamma_2 \sum_{m=1}^{M-1} \sum_{q=m+1}^M (r_{y_{m,q}} - r_{\hat{y}_{m,q}})^2, \end{aligned} \quad (\text{A4})$$

where the first term is the NLPD, the second term is the sum of squared differences between the observed and predicted site variances, and the third term is the sum of squared differences between the elements of the observed and predicted correlation matrices. The coefficients γ_1 and γ_2 control the relative scaling of the NLPD and the two constraint terms. In the current study, values of the γ coefficients are scaled following the first iteration of the minimization such that all terms in the cost function are weighted approximately equally. From Eq. (B2), applying separate constraints on the site variances and the intersite correlations is equivalent to applying a constraint on the covariances.

As mentioned above, the evaluation of \mathcal{L}'_E can be sped up by replacing variances–correlations calculated from the synthetic series \hat{y}_m with values calculated directly from the Bernoulli–gamma parameters. Predicted variances are given by

$$s_{\hat{y}_m} = \langle s_m^{(B)} \rangle + s_{\mu_m^{(B)}}, \quad (\text{A5})$$

where, from section 3b, the first term is the mean of the series of conditional variances, and the second term is the variance of the series of conditional means; $\langle \cdot \rangle$ denotes taking the temporal mean of a series. Likewise, values of the correlations are estimated from the series of conditional means $\mu_m^{(B)}$. After replacement, the final version of the cost function for the EBDN model is given by

$$\begin{aligned} \mathcal{L}_E^{(f)} = & -\sum_{t=1}^N \sum_{m=1}^M \log\{f_m[y_m(t)|x(t)]\} \\ & + \gamma_1 \sum_{m=1}^M (s_{y_m} - s_{\mu_m^{(B)}} - \langle s_m^{(B)} \rangle)^2 \\ & + \gamma_2 \sum_{m=1}^{M-1} \sum_{q=m+1}^M (r_{y_{m,q}} - r_{\mu_{m,q}^{(B)}})^2. \end{aligned} \quad (\text{A6})$$

Following the above substitutions, one problem still remains. The series of conditional means $\mu_m^{(B)}$ (see Fig. 6c) will tend to have smaller day-to-day variability than the synthetic series generated by sampling from the conditional Bernoulli–gamma distributions \hat{y}_m (see Fig. 6d). As a result, correlation estimates based on $\mu_m^{(B)}$ exhibit systematic biases with respect to those based on \hat{y}_m . A simple iterative correction algorithm is thus used to nudge the biased estimates toward more realistic values.

- i) The correction algorithm begins by finding ANN weights and biases that minimize the cost function $\mathcal{L}_E^{(f)}$ using values of $r_{y_{m,q}}$ from the observations and values of the predicted correlations $r_{\hat{y}_{m,q}}$ approximated by $r_{\mu_{m,q}^{(B)}}$.
- ii) Following the minimization, estimates of $r_{\hat{y}_{m,q}}$ are made from the trained EBDN based on multiple realizations of the synthetic precipitation series \hat{y}_m , which are generated by the process described in section 4b.
- iii) The differences between the observed and estimated values of the correlations $r_{y_{m,q}} - r_{\hat{y}_{m,q}}$ are then found and are added to the values of $r_{y_{m,q}}$, which results in adjusted values $r_{y_{m,q}^{(a)}}$ that are either lower or higher than those observed, depending on whether the bias in the modeled correlations is positive or negative.
- iv) The biases in the estimated correlations that result from replacing \hat{y}_m with $\mu_m^{(B)}$ are reduced by minimizing $\mathcal{L}_E^{(f)}$ again, this time with the adjusted correlations $r_{y_{m,q}^{(a)}}$ replacing the observed correlations $r_{y_{m,q}}$ in the third term of the cost function.
- v) Steps ii–iv are repeated, each time adding the current estimates of $r_{y_{m,q}} - r_{\hat{y}_{m,q}}$ to the previous values of the adjusted correlations $r_{y_{m,q}^{(a)}}$ and then minimizing $\mathcal{L}_E^{(f)}$.

To illustrate this process, an EBDN model with five hidden-layer nodes was trained on the data described in section 2. The model was initially trained for 100 iterations of the quasi-Newton minimization algorithm; each application of the correction algorithm involved running the minimization algorithm for another 20 itera-

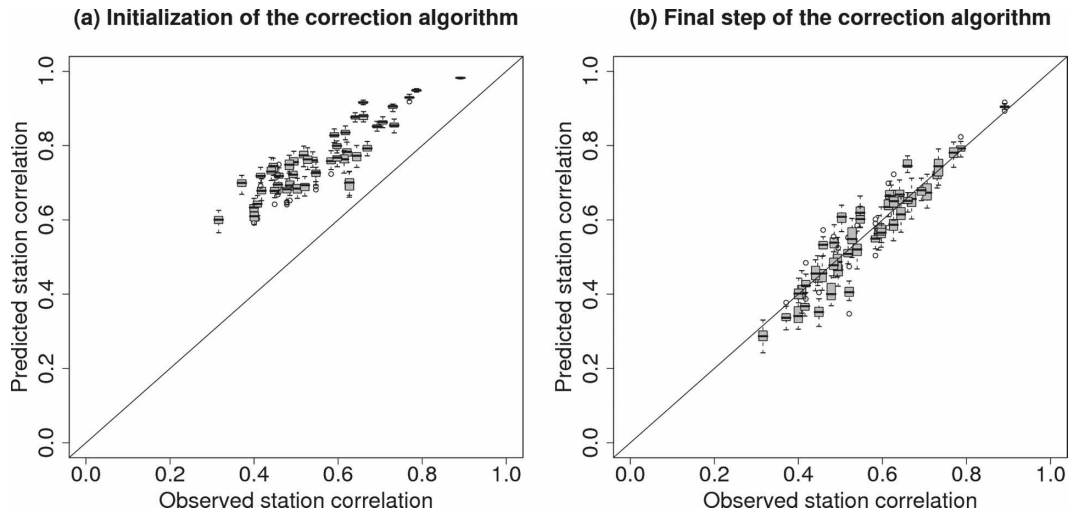


FIG. A1. Observed correlations vs boxplots of predicted correlations from 30 synthetic precipitation series following (a) the initialization of the correction algorithm and (b) the second and final iteration of the correction algorithm.

tions, each time starting from the previous weights and biases. Plots of observed correlations versus predicted correlations based on 30 realizations of \hat{y}_m from the trained model are shown in Fig. A1. Figure A1a shows the results following the initial minimization run. Without correction, the EBDN model overestimated the degree of spatial correlation between the sites, leading to a positive bias in the predicted correlations. Figure A1b shows the results following two applications of the correction algorithm. The correction algorithm successfully removed this bias, resulting in a model capable of representing the spatial variability between sites in a more realistic manner.

REFERENCES

- Bishop, C. M., 1995: *Neural Networks for Pattern Recognition*. Oxford University Press, 482 pp.
- Brankovic, C., and F. Molteni, 2004: Seasonal climate and variability of the ECMWF ERA-40 model. *Climate Dyn.*, **22**, 139–155.
- Buishand, T. A., and T. Brandsma, 2001: Multisite simulation of daily precipitation and temperature in the Rhine basin by nearest-neighbor resampling. *Water Resour. Res.*, **37**, 2761–2776.
- Bürger, G., 1996: Expanded downscaling for generating local weather scenarios. *Climate Res.*, **7**, 111–128.
- , 2002: Selected precipitation scenarios across Europe. *J. Hydrol.*, **262**, 99–110.
- , and Y. Chen, 2005: Regression-based downscaling of spatial variability for hydrologic applications. *J. Hydrol.*, **311**, 299–317.
- Cannon, A. J., cited 2007a: Multi-site precipitation downscaling via an expanded conditional density network. [Available online at doi:10.1038/npre.2007.446.1.]
- , 2007b: Nonlinear analog predictor analysis: A coupled neural network/analog model for climate downscaling. *Neural Networks*, **20**, 444–453.
- , and P. H. Whitfield, 2002: Downscaling recent streamflow conditions in British Columbia, Canada using ensemble neural network models. *J. Hydrol.*, **259**, 136–151.
- , —, and E. R. Lord, 2002: Synoptic map-pattern classification using recursive partitioning and principal component analysis. *Mon. Wea. Rev.*, **130**, 1187–1206.
- Caruana, R., 1997: Multitask learning. *Mach. Learn.*, **28**, 41–75.
- Cawley, G. C., M. R. Haylock, and S. R. Dorling, 2006: Predictive uncertainty in environmental modelling. *Proc. Int. Joint Conf. on Neural Networks*, Vancouver, BC, Canada, IEEE, 5347–5354.
- , G. Janacek, M. Haylock, and S. R. Dorling, 2007: Predictive uncertainty in environmental modelling. *Neural Networks*, **20**, 537–549.
- Charles, S. P., B. C. Bates, and J. P. Hughes, 1999: A spatiotemporal model for downscaling precipitation occurrence and amounts. *J. Geophys. Res.*, **104** (D24), 31 657–31 669.
- Dimopoulos, I., J. Chronopoulos, A. Chronopoulou-Sereli, and S. Lek, 1999: Neural network models to study relationships between lead concentrations in grasses and permanent urban descriptors in Athens city (Greece). *Ecol. Modell.*, **120**, 157–165.
- Dorling, S. R., R. J. Foxall, D. P. Mandic, and G. C. Cawley, 2003: Maximum likelihood cost functions for neural network models of air quality data. *Atmos. Environ.*, **37**, 3435–3443.
- Dunn, P. K., 2004: Occurrence and quantity of precipitation can be modelled simultaneously. *Int. J. Climatol.*, **24**, 1231–1239.
- Faucher, M., W. R. Burrows, and L. Pandolfo, 1999: Empirical-statistical reconstruction of surface marine winds along the western coast of Canada. *Climate Res.*, **11**, 173–190.
- Gangopadhyay, S., M. Clark, and B. Rajagopalan, 2005: Statistical downscaling using K -nearest neighbors. *Water Resour. Res.*, **41**, W02024, doi:10.1029/2004WR003444.
- Gardner, M. W., and S. R. Dorling, 1998: Artificial neural networks (the multilayer perceptron)—A review of applications in the atmospheric sciences. *Atmos. Environ.*, **32**, 2627–2636.

- Haylock, M. R., G. C. Cawley, C. Harpham, R. L. Wilby, and C. M. Goodess, 2006: Downscaling heavy precipitation over the United Kingdom: A comparison of dynamical and statistical methods and their future scenarios. *Int. J. Climatol.*, **26**, 1397–1415.
- Huth, R., J. Kysely, and M. Dubrovsky, 2001: Time structure of observed, GCM-simulated, downscaled, and stochastically generated daily temperature series. *J. Climate*, **14**, 4047–4061.
- Imbert, A., and R. E. Benestad, 2005: An improvement of analog model strategy for more reliable local climate change scenarios. *Theor. Appl. Climatol.*, **82**, 245–255.
- Mackay, D. J. C., 1998: Gaussian processes—A replacement for supervised neural networks? *Neural Networks and Machine Learning*, C. M. Bishop, Ed., NATO ASI Series, Vol. 168, Springer, 133–165.
- Mekis, E., and W. D. Hogg, 1999: Rehabilitation and analysis of Canadian daily precipitation time series. *Atmos.–Ocean*, **37**, 53–85.
- Rajagopalan, B., and U. Lall, 1999: A k -nearest-neighbor simulator for daily precipitation and other weather variables. *Water Resour. Res.*, **35**, 3089–3101.
- Salathe, E. P., 2005: Downscaling simulations of future global climate with application to hydrologic modelling. *Int. J. Climatol.*, **25**, 419–436.
- Schnabel, R. B., J. E. Koontz, and B. E. Weiss, 1985: A modular system of algorithms for unconstrained minimization. *ACM Trans. Math. Software*, **11**, 419–440.
- Schoof, J. T., and S. C. Pryor, 2001: Downscaling temperature and precipitation: A comparison of regression-based methods and artificial neural networks. *Int. J. Climatol.*, **21**, 773–790.
- , and S. M. Robeson, 2003: Seasonal and spatial variations of serial and cross-correlation matrices used by stochastic weather generators. *Climate Res.*, **24**, 95–102.
- Stahl, K., R. D. Moore, J. M. Shea, D. Hutchinson, and A. J. Cannon, 2008: Coupled modelling of glacier and streamflow response to future climate scenarios. *Water Resour. Res.*, **44**, W02422, doi:10.1029/2007WR005956.
- Uvo, C. B., J. Olsson, O. Morita, K. Jinno, A. Kawamura, K. Nishiyama, N. Koreeda, and T. Nakashima, 2001: Statistical atmospheric downscaling for rainfall estimation in Kyushu Island, Japan. *Hydrol. Earth Syst. Sci.*, **5**, 259–271.
- von Storch, H., 1999: On the use of “inflation” in statistical downscaling. *J. Climate*, **12**, 3505–3506.
- Wilby, R. L., and T. M. L. Wigley, 1997: Downscaling general circulation model output: A review of methods and limitations. *Prog. Phys. Geogr.*, **21**, 530–548.
- , O. J. Tomlinson, and C. W. Dawson, 2003: Multi-site simulation of precipitation by conditional resampling. *Climate Res.*, **23**, 183–194.
- , S. P. Charles, E. Zorita, B. Timbal, P. Whetton, and L. O. Mearns, 2004: *Guidelines for Use of Climate Scenarios Developed from Statistical Downscaling Methods*. Intergovernmental Panel on Climate Change, 27 pp. [Available online at <http://www.ipcc-data.org/guidelines/>.]
- Wilks, D. S., 1998: Multisite generalization of a daily stochastic precipitation generation model. *J. Hydrol.*, **210**, 178–191.
- , 2006: *Statistical Methods in the Atmospheric Sciences*. 2nd ed. Academic Press, 627 pp.
- , and R. L. Wilby, 1999: The weather generation game: A review of stochastic weather generator models. *Prog. Phys. Geogr.*, **23**, 329–357.
- Williams, P. M., 1998: Modelling seasonality and trends in daily rainfall data. *Advances in Neural Information Processing Systems 10*, M. I. Jordan, M. J. Kearns, and S. A. Solla, Eds., MIT Press, 985–991.
- Xu, C. Y., 1999: From GCMs to river flow: A review of downscaling methods and hydrologic modelling approaches. *Prog. Phys. Geogr.*, **23**, 229–249.
- Yates, D. S., S. Gangopadhyay, B. Rajagopalan, and K. Strzepek, 2003: A technique for generating regional climate using a nearest-neighbor algorithm. *Water Resour. Res.*, **39**, 1199, doi:10.1029/2002WR001769.
- Yuval, and W. W. Hsieh, 2002: The impact of time-averaging on the detectability of nonlinear empirical relations. *Quart. J. Roy. Meteor. Soc.*, **128**, 1609–1622.
- Zorita, E., and H. von Storch, 1999: The analog method as a simple statistical downscaling technique: Comparison with more complicated methods. *J. Climate*, **12**, 2474–2489.